Title
Contribution of particulate nitrate to airborne measurements of total reactive nitrogen

Journal
Journal of Geophysical Research D: Atmospheres, 110(15)

ISSN
0148-0227

Authors
Miyazaki, Y
Kondo, Y
Takegawa, N
et al.

Publication Date
2005-08-16

DOI
10.1029/2004JD005502

Contribution of particulate nitrate to airborne measurements of total reactive nitrogen

Y. Miyazaki,[1] Y. Kondo,[1] N. Takegawa,[1] R. J. Weber,[2] M. Koike,[3] K. Kita,[4] M. Fukuda,[1] Y. Ma,[5] A. D. Clarke,[6] V. N. Kapustin,[6] F. Flocke,[7] A. J. Weinheimer,[7] M. Zondlo,[8] F. L. Eisele,[2,7] D. R. Blake,[9] and B. Liley[10]

Received 10 October 2004; revised 15 April 2005; accepted 10 May 2005; published 12 August 2005.

[1] Simultaneous measurements of speciated, total reactive nitrogen (NO_y) and particulate NO_3^- (particle diameter <1.3 μm) were made on board the NASA P-3B aircraft over the western Pacific in February–April 2001 during the Transport and Chemical Evolution over the Pacific (TRACE-P) experiment. Gas-phase and particulate NO_y was measured using a gold tube catalytic converter. For the interpretation of particulate NO_y, conversion efficiencies of particulate NH_4NO_3, KNO_3, $NaNO_3$, and $Ca(NO_3)_2$ were measured in the laboratory. Only NH_4NO_3 showed quantitative conversion, and its conversion efficiency was as high as that for HNO_3. NO_y measured on board the aircraft was found to be systematically higher by 10–30% than the sum of the individual NO_y gas components ($\sum(NO_y)_i$) at 0–4 km. Particulate NO_3^- concentrations measured by a particle-into-liquid sampler (PILS) were nearly equal to $NO_y - \sum(NO_y)_i$ under low-dust-loading conditions. The PILS data showed that the majority of the particulate NO_3^- was in the form of NH_4NO_3 under these conditions, suggesting that NH_4NO_3 particles were quantitatively converted to detectable NO by the NO_y converter, consistent with the laboratory experiments. The contribution of particulate NO_3^- to NO_y was most important at 0–2 km, where NO_3^- constituted 10–30% of NO_y during TRACE-P. On average, the amounts of particulate NO_3^- and gas-phase HNO_3 were comparable in this region.

Citation: Miyazaki, Y., et al. (2005), Contribution of particulate nitrate to airborne measurements of total reactive nitrogen, *J. Geophys. Res.*, *110*, D15304, doi:10.1029/2004JD005502.

1. Introduction

[2] Reactive nitrogen species play a central role in determining the levels of ozone and hydroxyl radicals in the troposphere [e.g., *Crutzen*, 1979; *Liu et al.*, 1987; *Chameides et al.*, 1992]. Total reactive nitrogen (NO_y) in the troposphere is generally composed of NO, NO_2, peroxyacetyl nitrates (PANs), nitric acid (HNO_3), HONO, HO_2NO_2, NO_3, N_2O_5, organic nitrate, and particulate nitrate (NO_3^-). One of the major uncertainties in evaluating the budget of reactive nitrogen is due to a lack of fast response and accurate measurements of both gas-phase HNO_3 and particulate NO_3^-. This point is also important in evaluating loss rates of NO_y, because the deposition velocity for particulate NO_3^- with particle diameters (D_p) < 1 μm is 10 times smaller than that of gas-phase HNO_3 [*Warneck*, 1988].

[3] Reaction of NH_3 with HNO_3 produces ammonium nitrate (NH_4NO_3) particles generally with D_p < 1 μm. The thermodynamic equilibrium between HNO_3 and NH_4NO_3 shows a strong dependence on ambient temperature and relative humidity characteristic of the troposphere. Particulate NO_3^- with D_p > 1 μm can be produced by adsorption of HNO_3 on basic soil [*Wolff*, 1984] or sea-salt particles [*Savoie and Prospero*, 1982]. In the upper troposphere, HNO_3 uptake on cirrus ice cloud particles followed by gravitational settling may reduce the abundance of HNO_3 [*Lawrence and Crutzen*, 1998]. At high latitudes in the lower stratosphere, HNO_3 is irreversibly removed by sedimentation of large HNO_3-containing polar stratospheric cloud (PSC) particles (denitrification) formed at very low temperatures [*Solomon et al.*, 1986]. Therefore it is important to assess the contribution of particulate NO_3^- to NO_y in order to understand distributions of reactive nitrogen.

[1]Research Center for Advanced Science and Technology, University of Tokyo, Tokyo, Japan.
[2]School of Earth and Atmospheric Sciences, Georgia Institute of Technology, Atlanta, Georgia, USA.
[3]Earth and Planetary Science, Graduate School of Science, University of Tokyo, Tokyo, Japan.
[4]Department of Environmental Science, Ibaraki University, Mito, Ibaraki, Japan.
[5]Department of Civil and Environmental Engineering, Duke University, Durham, North Carolina, USA.
[6]School of Ocean and Earth Science and Technology, University of Hawaii at Manoa, Honolulu, Hawaii, USA.
[7]National Center for Atmospheric Research, Boulder, Colorado, USA.
[8]Southwest Sciences, Inc., Santa Fe, New Mexico, USA.
[9]Department of Chemistry, University of California, Irvine, California, USA.
[10]National Institute of Water and Atmospheric Research, Lauder, New Zealand.

0148-0227/05/2004JD005502

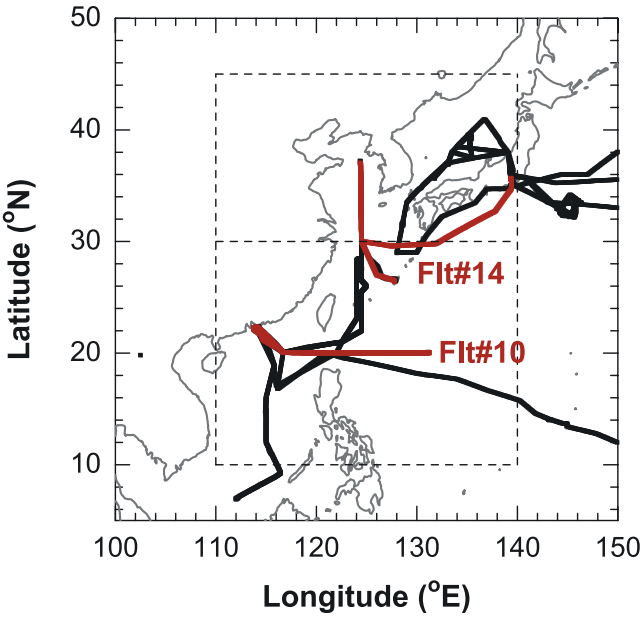

Figure 1. Flight tracks near the Asian continent during TRACE-P and regions where flights 10 and 14 were made (see text for details).

[4] To date, a number of attempts have been made to quantify the budget of NO_y over a variety of regions. Catalytic conversion of NO_y compounds on the surface of a heated gold tube, followed by chemiluminescence detection of NO [*Fahey et al.*, 1985] has been widely used for airborne measurements, because of its fast response and high sensitivity [e.g., *Hübler et al.*, 1992; *Ridley et al.*, 1994; *Sandholm et al.*, 1994; *Kondo et al.*, 1997a]. Over the western Pacific, NO_x, PAN, and HNO_3 obtained by airborne measurements together accounted for 90% of concurrently measured NO_y up to 7 km [*Kondo et al.*, 1997b]. Measurements of NO_y and the sum of reactive nitrogen species in the upper troposphere over the North Atlantic [*Talbot et al.*, 1999] showed that 90% of the measured NO_y was accounted for by measurements of the individual NO_y species.

[5] Over the North American continent in summer, aircraft measurements showed that the individually measured species (NO_x + HNO_3 + PANs + C_1-C_5 alkyl nitrate) constituted more than 90% of the measured NO_y on average at altitudes up to 7 km [*Neuman et al.*, 2002; *Ryerson et al.*, 2003; *Parrish et al.*, 2004]. They concluded that the sum of the individual NO_y constituents agreed with the measured NO_y within the instrument uncertainties over the region. *Day et al.* [2003] recently showed that the sum of total alkyl nitrates ($RONO_2$) routinely accounted for 10–20% of NO_y, using annual ground-based measurements at a rural site in California.

[6] In situ aircraft measurements of NO_y have been made through forward and/or rearward facing inlets. NO_y measured through forward facing inlets represents amplified particulate NO_y plus gas-phase NO_y. *Fahey et al.* [2001] observed large, HNO_3-containing particles with D_p = 10–20 μm in the winter Arctic lower stratosphere by in situ aircraft measurements of NO_y. Similarly, NO_y contained in cirrus cloud ice particles has been measured in the upper troposphere [*Weinheimer et al.*, 1998; *Kondo et al.*, 2003] and in the lowermost stratosphere [*Feigl et al.*, 1999]. However, the response of NO_y measurement techniques or their sampling systems to particulate NO_3^- in the lower troposphere is not fully understood. In particular, a quantitative assessment of the contribution of particulate NO_3^- to NO_y sampled through rearward facing inlets has not been made on airborne platforms in the lower troposphere. The major uncertainties are (1) particle collection efficiency of the rearward facing inlet and (2) conversion efficiency of particulate NO_3^- in the NO_y converter.

[7] In this paper, we present evidence of the detection of particulate NO_3^- by an airborne NO_y instrument during the NASA Transport and Chemical Evolution over the Pacific (TRACE-P) experiment. We focus on evaluating the contribution of NO_3^- to NO_y measurements over the western Pacific.

2. Experiment

[8] During the TRACE-P experiment (February–April 2001), NO_y and individual NO_y compounds were measured on board the P-3B aircraft over the Pacific at 0–7 km [*Kondo et al.*, 2004]. We use the data obtained in the region of 10°–45°N, 110°–140°E, where most of the P-3B sampling was made (Figure 1). The data used in this study were obtained during flights 10–20 (9 March to 4 April 2001). Since details of each measurement technique are summarized elsewhere [see *Miyazaki et al.*, 2003, Table 1], we describe here the NO_y and aerosol measurements.

2.1. Gas-Phase and Particulate NO_y

[9] NO_y was measured using an NO-O_3 chemiluminescence technique combined with a gold tube heated to 300°C with addition of CO, catalytically converting NO_y compounds into NO [*Kondo et al.*, 1997a]. The NO_y converter unit was mounted on the side of the window plate inside the aircraft cabin to minimize the length of the inlet tubes. During in-flight calibrations, known concentrations of NO and NO_2 in N_2 were added into the sample air to calibrate the absolute sensitivity and conversion efficiency. The estimated uncertainty of the NO mixing ratios of the calibration gas was 2%, and the uncertainty of the flow rates was estimated to be ±2%. The error from the artifact for NO_y is estimated to be ±2% for NO_y mixing ratios of 500 parts per trillion by volume (pptv). The HNO_3 conversion efficiency was higher than 95%, which was determined by both laboratory tests and in-flight calibration during the previous aircraft missions [*Kondo et al.*, 1997a; *Koike et al.*, 2000]. It was measured to be stable over time within ±5% [*Kondo et al.*, 1997a]. The conversion efficiencies of HCN and CH_3CN were 2% and 1–2%, respectively [*Koike et al.*, 2000]. From the observed values of HCN (<220 pptv) and CH_3CN (<150 pptv) at 0–6 km during TRACE-P [*Singh et al.*, 2003], the uncertainty associated with the conversion of these species is estimated to be less than 2%. Overall, the accuracy of the NO_y measurement was estimated to be ±13%.

[10] In this study, ΔNO_y is defined as the difference between the measured NO_y and $\sum(NO_y)_i$,

$$\Delta NO_y = NO_y - \sum (NO_y)_i \quad (1)$$

Table 1. Approximate Stokes Numbers Calculated for the P-3B NO_y Inlet at a Pressure Altitude of 950 hPa

	Value
D_p = 0.3 μm	0.01
D_p = 0.5 μm	0.03
D_p = 1.0 μm	0.09
D_p = 1.5 μm	0.19

where $\sum(NO_y)_i$ is defined as the sum of individually measured gas-phase NO_y compounds.

$$\sum(NO_y)_i = NO + NO_2 + HNO_3 + PAN + PPN + C_1\text{-}C_5 \text{ alkyl nitrates} \quad (2)$$

The uncertainties of $\sum(NO_y)_i$ and ΔNO_y were estimated to be ±14% and ±32%, respectively, by combining possible errors of the individual instruments.

[11] During TRACE-P, two NO_y inlets were located on the right window plate of the cabin, one facing rearward and the other facing forward. The inlet of the NO_y instrument was made of 3/8-inch outer diameter Teflon tubing heated to 50°C for rearward and 100°C for forward upstream of the NO_y converter unit. The tubing from the inlet to the gold tube converter is not straight but is curved (angle 90 deg, radius 5 cm). In order to estimate the collection efficiency of particles for the rearward NO_y inlet, we made a simple calculation based on the Stokes number, which is the ratio of a particle's "persistence" to the size of the obstacle, often used to characterize inertial impaction. The rearward facing inlet allows the collection of particles with Stokes numbers less than about 0.2, which track streamlines of sample air because of their negligibly small inertia. At Stokes numbers greater than 0.2, particles do not follow the streamlines that curve into the rearward facing inlet. Approximate Stokes numbers were estimated for the P-3B NO_y sampling inlet by a simple aerodynamical calculation (Table 1). On the basis of these calculations, we estimated that the NO_y inlet discriminates against particles with D_p larger than 1.5 and 1.1 μm at altitudes of 0.5 and 6 km, respectively. The collection efficiency of particles with D_p > 1.5 μm is estimated to be almost zero. It should be noted that effects of turbulence were not taken into account in the above estimate. Turbulence introduces uncertainties in the estimate of the cutoff size, although they are not quantified in this work.

[12] During TRACE-P, NO_y was also sampled through a forward facing inlet using an independent detection channel. The forward facing inlet was subisokinetic and collected particles including those with D_p > 1.5 μm that were unlikely sampled by the rearward NO_y inlet. The NO_y measured through the forward facing inlet (NO_y (f)) represents the sum of gas-phase NO_y and amplified particulate NO_3^-. When particulate NO_3^- is absent, NO_y signals from NO_y (f) and NO_y are identical. When encountered, particulate NO_3^- including larger particles (D_p > 1.5 μm), NO_3^- (L), can be defined as follows:

$$NO_3^-(L) = \left(NO_y(f) - \sum(NO_y)_i\right)/EF \quad (3)$$

EF represents the enhancement factor for the forward facing inlet, which depends on the size of the particles due to subisokinetic sampling [*Fahey et al.*, 1989].

2.2. Laboratory Experiments

[13] In order to estimate the conversion efficiency of particulate NO_3^- in the gold tube converter, we conducted laboratory experiments using an aerosol generation system (Figure 2). Because particulate NO_3^- is observed typically in the form of NH_4NO_3, KNO_3, $NaNO_3$, and $Ca(NO_3)_2$ in the troposphere, we measured the conversion efficiencies of the particles in these forms in the laboratory. Dry particles made of these chemical compositions were generated using an atomizer (TSI model 3076) and diffusion dryer. A differential mobility analyzer (DMA) (TSI model 3080) was used to produce monodisperse particles with a size range between 300 and 400 nm. The number concentrations were monitored by a condensation particle counter (CPC) (TSI model 3022A). Mass concentrations of nitrate particles were calculated using the density (ρ), diameter, number concentrations, and shape factor [*Jayne et al.*, 2000; *DeCarlo et al.*, 2004]. The results are summarized in Table 2. The conversion efficiency for NH_4NO_3 was 91 ± 9% at NO_3^- mixing ratios of 2000–5000 pptv. The derived conversion efficiency for particulate NH_4NO_3 was as high as that for HNO_3. The difference between the two conversion efficiencies is to within the measurement uncertainties. Uncertainties of the

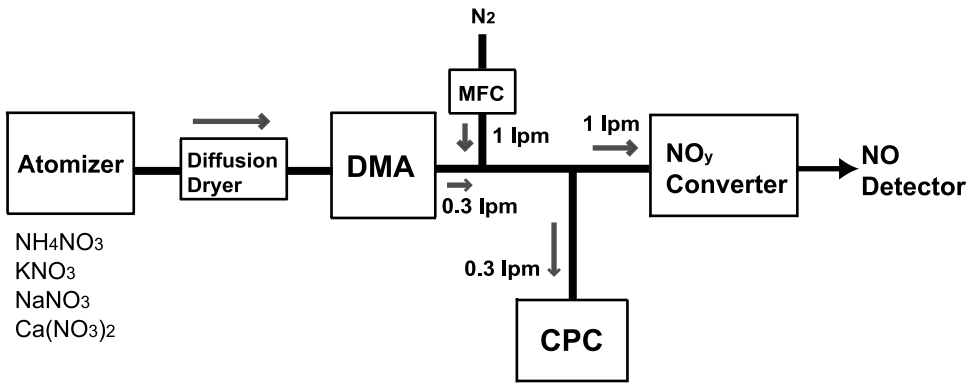

Figure 2. Schematic of the laboratory setup to generate and measure particulate NO_3^-. The number concentration of generated aerosol was measured by a condensation particle counter (CPC).

Table 2. Conversion Efficiencies of Particulate NO_3^- Species Measured in the Laboratory[a]

	NH_4NO_3	KNO_3	$NaNO_3$	$Ca(NO_3)_2$
NO_3^- Conversion Efficiency, %	90.7 ± 9.0	1.2 ± 0.5	2.0 ± 0.3	3.4 ± 0.8
Assumed Density ρ, g/cm^3	1.72	2.11	2.66	2.36
Boiling point/Melting point, °C	210 (b)	334 (m)	380 (b)	561 (m)

[a]The assumed density and boiling/melting points for different forms of particles are also shown. Here, "(b)" and "(m)" denote boiling point and melting point, respectively.

NH_4NO_3 conversion efficiency due to evaporation of NH_4NO_3 particles in the inlet system are small. The residence time of particulate NO_3^- between the atomizer and NO_y converter is about 1 s, which is much shorter than the typical timescale of a few minutes required for evaporation of particulate NO_3^- [e.g., *Neuman et al.*, 2003]. In fact, our recent ground-based measurements showed that the ambient HNO_3 concentrations were smaller than 8% of the particulate NO_3^- levels (~1 ppbv) during nighttime, when the ambient temperature was about 15°C (K. Kita et al., A chemical ionization mass spectrometer for ground-based measurement of nitric acid, submitted to *Journal of Atmospheric and Oceanic Technology*, 2005), which is similar to the room air temperature during the laboratory experiments. By contrast, the conversion efficiencies for KNO_3, $NaNO_3$, and $Ca(NO_3)_2$ were as low as 1.2 ± 0.5%, 2.0 ± 0.3%, and 3.4 ± 0.8%, respectively.

[14] These results are consistent with the boiling or melting points of the particulate NO_3^- species (Table 2). NH_4NO_3 (boiling point 210°C) should be vaporized at the temperature of the NO_y converter (300°C). On the other hand, the melting or boiling points of KNO_3, $NaNO_3$, and $(Ca(NO_3)_2)$ are higher than the temperature of the NO_y converter, leading to significantly low conversion efficiencies.

2.3. Aerosol Measurements

[15] Aerosol chemical composition (NO_3^-, SO_4^{2-}, Cl^-, NH_4^+, Na^+, K^+, and Ca^{2+}) was measured every 4 min, using a particle-into-liquid sampler coupled with ion chromatography analysis (PILS-IC) [*Weber et al.*, 2001; *Orsini et al.*, 2003]. The PILS employs a steam saturator to grow the aerosol to sizes that result in liquid impaction followed by measurement of the major ions using IC. For the PILS, the collection efficiency for $D_p < 0.7$ μm was estimated to be 90%, decreasing to ~50% for $D_p = 1.3$ μm (upper size cut), which was determined by laboratory calibration [*Ma et al.*, 2004]. The efficiency for $D_p > 3$ μm was nearly zero. The uncertainty of the NO_3^- measurement was estimated to be ±15%. The P-3B used a shrouded inlet for the aerosol measurements, which maintained an attack angle independent of turbulence characteristics in the diffuser cone [*Clarke et al.*, 2004]. The aerosol inlet was kept isokinetic during flight by adjusting flow rates as flight parameters changed.

[16] Upper size cuts of the NO_y and PILS systems are shown in Figure 3. Basically, the size cutoff of the PILS is similar to that of the NO_y instrument. However, the PILS measures particles within a size range of $D_p = 1.5-3$ μm, although the collection efficiency within this range is less than 50%. On the other hand, it is unlikely that particles with $D_p = 1.5-3$ μm were sampled by the NO_y instrument. We discuss the difference in the threshold of particle size in section 4.

[17] Ambient aerosol size distributions were measured by a laser optical counter (OPC, PMS LAS-X, Boulder, CO) [*Clarke et al.*, 2004]. The OPC provided size distributions of "dry" (heated to 40°C) particles between 0.1 and 20.0 μm. The terms "fine particle" and "coarse particle" in this paper are defined as particles within size ranges of $D_p < 1$ μm and $D_p > 1$ μm, respectively. Ambient wet particle size distributions are estimated by assuming that particles with $D_p < 0.6$ μm absorb water as a typical marine boundary layer aerosol [*Swietlicki et al.*, 2000], and particles with $D_p > 0.6$ μm are treated as dust and do not absorb water [*Weber et al.*, 2003]. All of the P-3B data were merged into the time interval of aerosol sampling (~4 min).

3. Particulate NO_3^- Detected by the NO_y Instrument

[18] Figure 4 shows time series plots of NO_y, ΔNO_y, NO_3^-, fine-particle volume, NH_4^+, and K^+ obtained on 9 March (flight 10) and 18 March (flight 14) 2001. The flight tracks are also shown in Figure 1. A large enhancement of NO_y up to 2500 pptv was observed at an altitude of 3 km during flight 10. The ΔNO_y and NO_3^- concentrations reached their maximum values in the same air masses. An interesting feature is that K^+ also showed its maximum (~900 pptv) in these plumes, which were identified as originating from biomass burning in southeast Asia by using back trajectories and satellite fire maps [*Ma et al.*, 2003; *Kondo et al.*, 2004]. *Ma et al.* [2003] used observed K^+/sulfate ratios to infer that 30% of total aerosol mass in Asian pollution plumes sampled

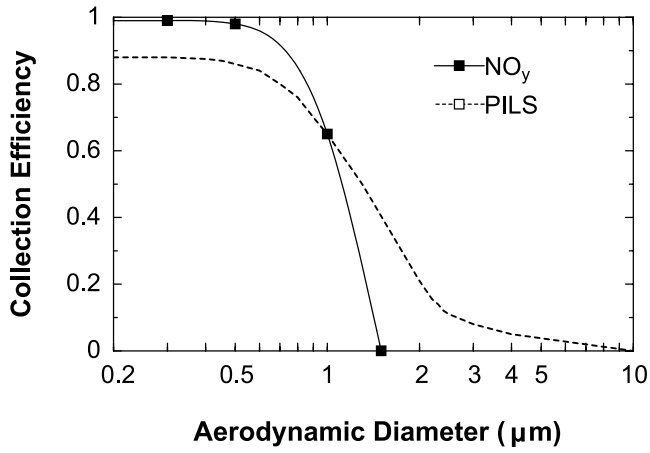

Figure 3. Upper size limits of particle measurements for the NO_y and PILS instruments. The NO_y transmission curve was derived on the basis of the calculated Stokes number assuming no turbulence. Turbulence introduces uncertainties in the estimate of the cutoff size, although they are not quantified in this work. The transmission curve for the PILS was determined experimentally by generating monodisperse calibration particles using a nebulizer/DMA and vibrating-orifice aerosol generator in the laboratory [*Ma et al.*, 2004].

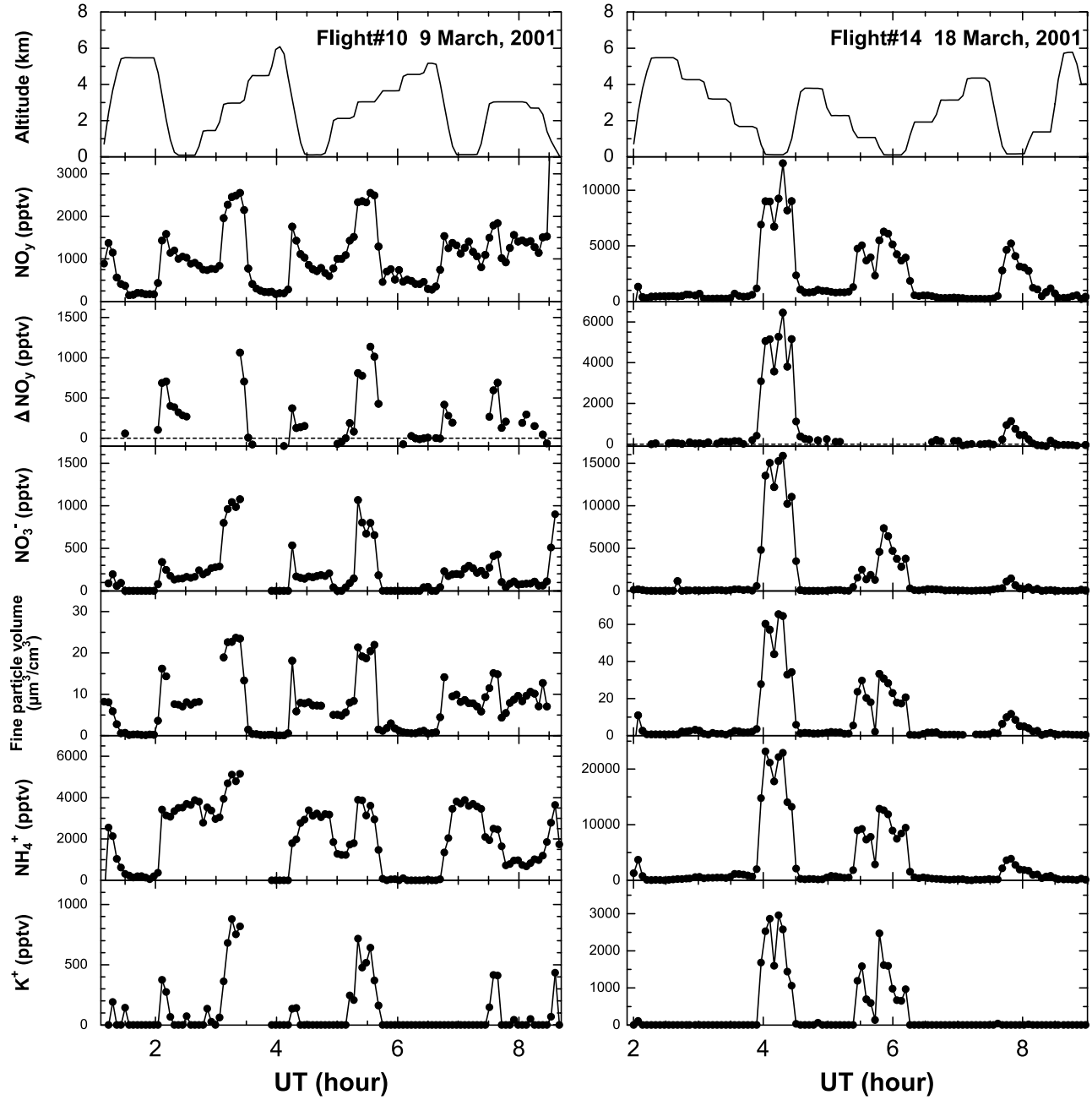

Figure 4. Time series plots for flight 10 and flight 14 with altitude, NO_y, ΔNO_y, NO_3^-, fine-particle volume, NH_4^+, and K^+.

during TRACE-P originated from biomass or biofuel burning. During flight 14, very distinct plumes were observed and all species reached their highest concentrations at 0–1 km over the Yellow Sea (34°–36°N, see Figure 1). Peak concentrations for NO_y, ΔNO_y, and NO_3^- were 13,000, 6500, and 16,000 pptv, respectively. For both cases, fine-particle volumes were also enhanced (25–70 $\mu m/cm^3$) in these plumes.

[19] In order to evaluate the contribution of NO_3^- to ΔNO_y, their correlations at 0–4 km are shown in Figure 5. A majority of the NO_3^- and ΔNO_y (<2500 pptv) data points in Figure 5a lie along the 1:1 line, within the error bars, indicating that NO_3^- measured by the PILS-IC can account for the ΔNO_y. In Figure 5b, data points with ΔNO_y > 2500 pptv are also shown according to Ca^{2+} concentration. Ca^{2+} is generally considered to be derived from soil and crustal material and thus can be used as a tracer for dust. For the data with ΔNO_y < 2500 pptv, which accounted for 97% of all the data points, dust loadings were low ($[Ca^{2+}]$ < 200 pptv). On the other hand, NO_3^- with ΔNO_y > 2500 pptv far exceeded ΔNO_y where dust loadings were high ($[Ca^{2+}]$ > 400 pptv). These data with ΔNO_y > 2500 pptv were all obtained over the Yellow Sea during flight 14 (Figure 4). A possible explanation of the excess NO_3^- relative to ΔNO_y is discussed in section 4.

[20] Figure 6 shows latitudinal distributions of (coarse-particle volume)/(fine-particle volume) ratios observed at 0–4 km during TRACE-P. Although variability was large,

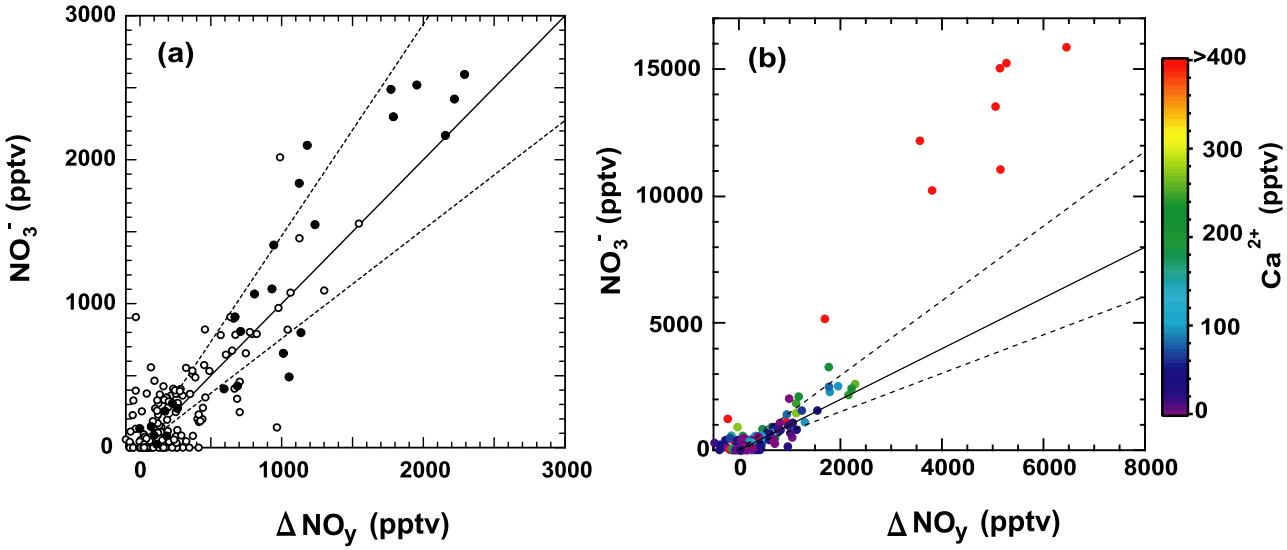

Figure 5. Linear relationship between particulate NO_3^- and ΔNO_y observed at 0–4 km for all flights during the TRACE-P period. Solid and dashed lines indicate the 1:1 line and the uncertainty of ΔNO_y, respectively. (a) Solid circles indicate the data in which NO_3^- + SO_4^{2-} and NH_4^+ in equivalence balanced to within ±30%. (b) The data points are color-coded according to the concentration of nss-Ca^{2+}. Note that Figure 5a is a subset of the data points in Figure 5b and that the scales of the *x* and *y* axes in both figures are different.

the median ratio at 10°–30°N was lower than 1, suggesting that a majority of particles was in the fine mode ($D_p < 1$ μm), likely in biomass burning plumes [*Kondo et al.*, 2004]. A dominance of fine particles in biomass burning plumes was previously observed, for instance, in Brazil [*Reid and Hobbs*, 1998]. By contrast, at 30°–45°N, coarse-particle volume was larger than fine-particle volume. Air masses with a large abundance of coarse particles observed in this region were heavily influenced by dust [*Jordan et al.*, 2003a]. In fact, *Jordan et al.* [2003a] found that dust particles accounted for 77% of the total aerosol mass in the Chinese low-altitude outflow, typically observed at 30°–45°N during TRACE-P. Figure 7 presents a plot of the $NO_3^-/\Delta NO_y$ ratio versus the (coarse-particle volume)/(fine-particle volume) ratio. At the $NO_3^-/\Delta NO_y$ ratio close to 1, fine-particle volume was generally larger than coarse-particle volume and dust loadings were low with $[Ca^{2+}] <$ 200 pptv. These results suggest that a majority of ΔNO_y can be attributed to fine particles.

[21] Contributions of NO_y species not measured in this study to ΔNO_y are not significant in this study. Model calculations [*Brasseur et al.*, 1999; *Talbot et al.*, 1999] indicate that HO_2NO_2 is the most abundant unmeasured NO_y species. However, it is thermally stable only at the cold temperatures of the upper troposphere, and the HO_2NO_2/NO_y ratio is estimated to be lower than 0.01 below 4 km [*Brasseur et al.*, 1999]. On the other hand, ΔNO_y is significantly large in the lower troposphere (0–4 km) in this case. Consequently, the contribution of HO_2NO_2 to ΔNO_y can be negligible in this study.

4. Chemical Form of Particulate NO_3^-

[22] In this section, we infer the chemical form of particulate NO_3^- detected by the NO_y instrument. Figure 8 shows average ionic composition at 0–4 km with ΔNO_y both less than and greater than 2500 pptv, where dust loadings were low with $[Ca^{2+}] <$ 200 pptv and high with $[Ca^{2+}] >$ 400 pptv, respectively. NH_4^+ was the main neutralizing agent of the acidic aerosol species, which accounted for 82 and 73% of the total cations with $\Delta NO_y <$ 2500 pptv and $\Delta NO_y >$ 2500 pptv, respectively. NH_4NO_3 forms by condensation of gas-phase HNO_3 with available NH_3 once all SO_4^{2-} is neutrized [*Seinfeld and Pandis*, 1998]. In order to examine this, the relationship between NO_3^- and NH_4^+ minus SO_4^{2-} in equivalence is shown in Figure 9. Overall, a

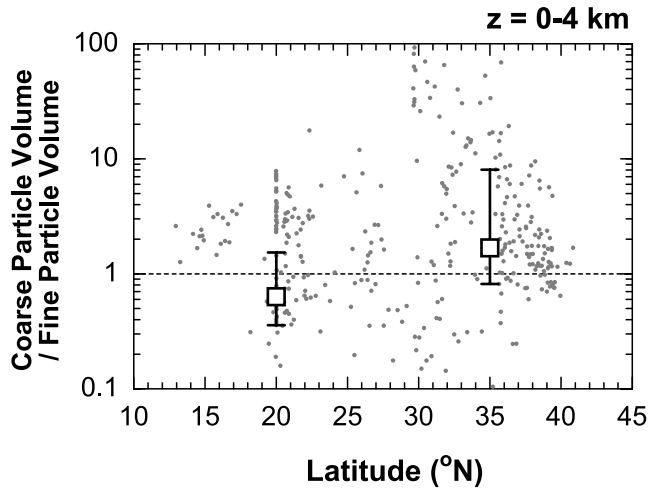

Figure 6. Latitudinal distributions of coarse (D_p = 1–20 μm)/fine (D_p = 0.1–1 μm) particle volume observed at 0–4 km. Median values are shown for 10°–30°N and 30°–45°N. The data points with fine-particle volume <0.2 $\mu m^3/cm^3$ are not used.

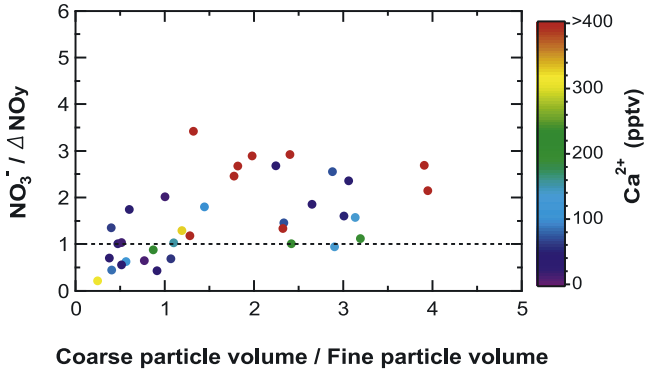

Figure 7. Relationship between $NO_3^-/\Delta NO_y$ and coarse (D_p = 1–20 μm)/fine (D_p = 0.1–1 μm) particle volume observed at 0–4 km. The data points are color-coded according to the concentration of nss-Ca^{2+}. Dashed lines indicate that the $NO_3^-/\Delta NO_y$ ratio is 1. The data points with ΔNO_y < 100 pptv and fine-particle volume <0.2 $\mu m^3/cm^3$ are not used.

positive correlation (r^2 = 0.77) with a slope of 1.10 shows that ion balance between NH_4^+ minus SO_4^{2-} and NO_3^- in equivalence is nearly complete, within 10% on average, suggesting available NH_3 to form NH_4NO_3. For ΔNO_y < 2500 pptv, the slope was 0.97 with r^2 = 0.66 and 1.34 with r^2 = 0.74 for ΔNO_y > 2500 pptv. The data for which NO_3^- + SO_4^{2-} and NH_4^+ in equivalence balanced within ±30% are plotted in Figure 5a (solid circles). The slope for the data points was 1.16 (r^2 = 0.87), lying close to the 1:1 line within the error bars, indicating that NH_4NO_3 was detected by the NO_y instrument.

[23] In order to estimate the relative contribution of cations other than NH_4^+ associated with NO_3^-, we consider the relative amounts of Ca^{2+}, K^+, and Na^+ by using PILS chemical composition data. If we assume that all of the Ca^{2+} and K^+ take up SO_4^{2-}, measured NO_3^- is considered to be in the form of NH_4NO_3, that is, NO_3^- as NH_4NO_3 = NH_4^+ – SO_4^{2-} in equivalence (upper limit). By contrast, when all Ca^{2+} and K^+ are assumed to take up the measured NO_3^-, the amount of NO_3^- as NH_4NO_3 can be derived from NO_3^- – (Ca^{2+} + K^+) in equivalence (lower limit). Considering these two limiting cases for NH_4NO_3, the amount of Ca^{2+} plus K^+ in equivalence is 44% of NO_3^- for the data points with ΔNO_y < 2500 pptv. Thus, when Ca^{2+} and K^+ are taken into account, the lower limit of NH_4NO_3 was estimated to be 56% of the total NO_3^-.

[24] For ΔNO_y < 2500 pptv, the correlation between Cl^- and Na^+ showed a slope of 1.35 with r^2 = 0.78 (not shown), close to the seawater ratio of 1.16. Moreover, Mg^{2+} showed a correlation with Na^+ (r^2 = 0.64) with a slope of 0.13, very close to their seawater ratio of 0.11, suggesting that sea-salt particles partly contributed to these species. A Cl^-/Na^+ ratio lower than the seawater ratio indicates acidification of particles by HNO_3, resulting in a Cl^- deficit to form $NaNO_3$. By using these data points, $NaNO_3$ was estimated to contribute <12% of NO_3^- for ΔNO_y < 2500 pptv. Overall, more than 44% of particulate NO_3^- (ΔNO_y < 2500 pptv) was estimated to be in the form of NH_4NO_3.

[25] On the other hand, for ΔNO_y > 2500 pptv, the ion balance between NO_3^- and NH_4^+ – SO_4^{2-} (open circles in Figure 9) and the relative abundance of Ca^{2+} + K^+ compared to NO_3^- (Figure 8) suggest that more than 70% of the observed NO_3^- was in the form of NH_4NO_3. In this case, the contribution of $NaNO_3$ was negligible (<1%).

[26] For the data points with ΔNO_y > 2500 pptv (<3% of the total), however, NO_3^- (7500–12,000 pptv) far exceeded the 1:1 line relative to ΔNO_y (Figure 5b). As stated in section 2, there are two possible explanations for the excess NO_3^-, defined as δNO_3^-:

$$\delta NO_3^- = NO_3^- - \Delta NO_y \quad (4)$$

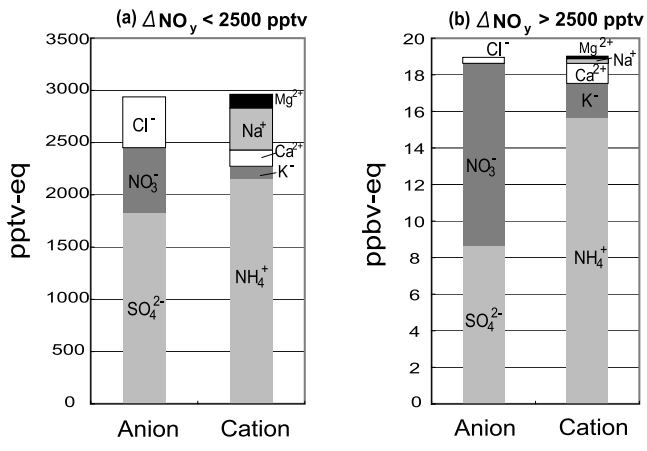

Figure 8. Ionic composition in pptv-equivalent with ΔNO_y (a) <2500 pptv and (b) >2500 pptv at 0–4 km. Note that the full scales of the *y* axes are different in Figures 8a and 8b.

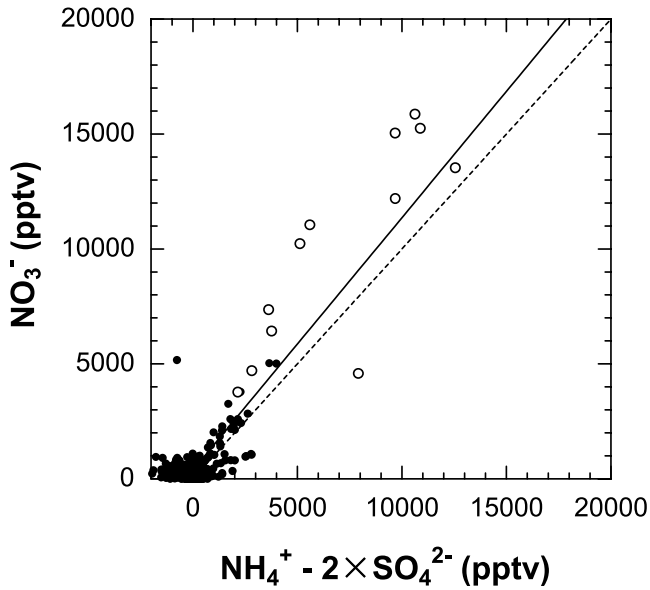

Figure 9. Relationship between NO_3^- and NH_4^+ minus SO_4^{2-} in equivalence. The solid line represents the least squares best fit, with a slope of 1.10. The dashed line indicates the 1:1 line. Open circles correspond to the data with high concentrations of Ca^{2+} (>400 pptv) obtained at 0–2 km over the Yellow Sea during flight 14.

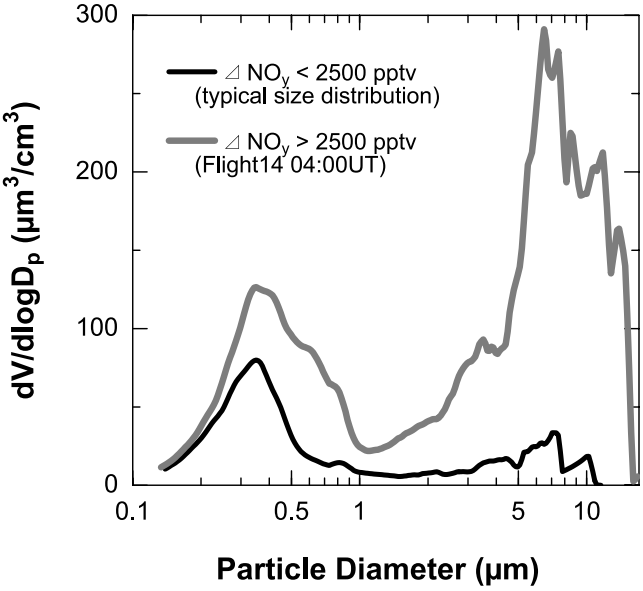

Figure 10. Typical size distributions representative of particles with $\Delta NO_y < 2500$ pptv (black line) and within the plumes with $\Delta NO_y > 2500$ pptv at 0400 UTC during flight 14 (gray line) measured by the OPC. The size distributions are calculated from number distributions for particles grown at ambient relative humidity, assuming that uptake is by dust particles.

(1) particles were not sampled by the NO_y instrument but were by the PILS-IC, because of their sizes, with $D_p = 1.5–3$ μm in the different inlet systems, and (2) particles were measured as water-soluble ions by the PILS-IC but not converted to measurable NO in the NO_y instrument (i.e., $Ca(NO_3)_2$ and KNO_3). We explore these two possibilities in detecting particulate NO_3^- by the NO_y instrument and the PILS-IC system.

[27] Regarding particle size, the data points where $NO_3^-/\Delta NO_y$ ratios exceed 1 (Figure 7), where coarse-particle volume tends to be larger relative to fine-particle volume under the high concentrations of Ca^{2+} (>400 pptv), are indicative of dust loading. *Jordan et al.* [2003b] used the DC-8 aircraft data for TRACE-P and showed that the dust was generally mixed with pollution and that a large fraction of nitrate was taken up by dust particles in the coarse mode, presumably through displacement of carbonate. Figure 10 shows OPC size distributions at ambient relative humidity with $\Delta NO_y > 2500$ pptv and typical distributions representative of particles for $\Delta NO_y < 2500$ pptv. The size distributions of particles with $\Delta NO_y < 2500$ pptv show that particles reside mostly in the fine mode ($D_p < 1$ μm), while the abundance in the coarse mode ($D_p > 1$ μm) is minimal. On the other hand, the distributions of particles with $\Delta NO_y > 2500$ pptv were characterized by the bimodal peaks within fine and coarse modes. On the basis of the size distributions and the PILS correction efficiency, we can roughly estimate that particles with $D_p = 1.5–3$ μm could contribute to about 10% of the total volume of particles collected by the PILS for $\Delta NO_y > 2500$ pptv.

[28] We further examined particulate NO_3^- containing the 1.5–3-μm range by using the NO_y (f) data. Figure 11 shows the relationship between NO_3^- and NO_3^- (L) (equation 3). Using the empirical expression given by *Durham and Lundgren* [1980], EF was estimated to be 2 for $D_p = 1.5$ μm, by assuming a particle density of 1.8 g cm^{-3} estimated from the OPC data. As stated in section 2, NO_3^- (L) represents particulate NO_3^- including larger particles ($D_p > 1.5$ μm), mainly as NH_4NO_3, which can be detected by the NO_y instrument. Considering that the EF range is 2 ± 0.5 for particles with $D_p = 0.5–3$ μm, the estimated uncertainty of NO_3^- (L) is given as +40%/−30%. For $\Delta NO_y < 2500$ pptv, NO_3^- showed agreement with NO_3^- (L), including particles that were not efficiently detected by the rearward NO_y system, indicating that almost all of δNO_3^- can be explained by NO_3^- (L). For $\Delta NO_y > 2500$ pptv, although it is difficult to evaluate the contribution of NO_3^- (L) to δNO_3^- because of the uncertainty of the EF, we estimate that approximately 20 ± 10% of δNO_3^- can be explained by NO_3^- (L). The amount of NO_3^- (L) in this case corresponds to 10% of the PILS NO_3^- in mass, which agrees well with the estimate from the particle volume by OPC (Figure 10), if the particle density is assumed to be constant.

[29] One of the possible reasons for the NH_4NO_3 particle size to reside in larger sizes ($D_p = 1.5–3$ μm) is that the relative humidity of the ambient air was relatively high, causing particles to absorb water before sampling. However, there is no clear relationship between the $NO_3^-/\Delta NO_y$ ratios and ambient relative humidity (not shown). Moreover, whether these particles were internally or externally mixed in the dust particles cannot be identified from these data alone.

[30] The sum of Ca^{2+} and K^+ in equivalence is plotted against δNO_3^- for $\Delta NO_y > 2500$ pptv in Figure 12. They are tightly correlated ($|r|^2 = 0.93$), indicating that δNO_3^- is partly associated with dust particles. In the current analysis,

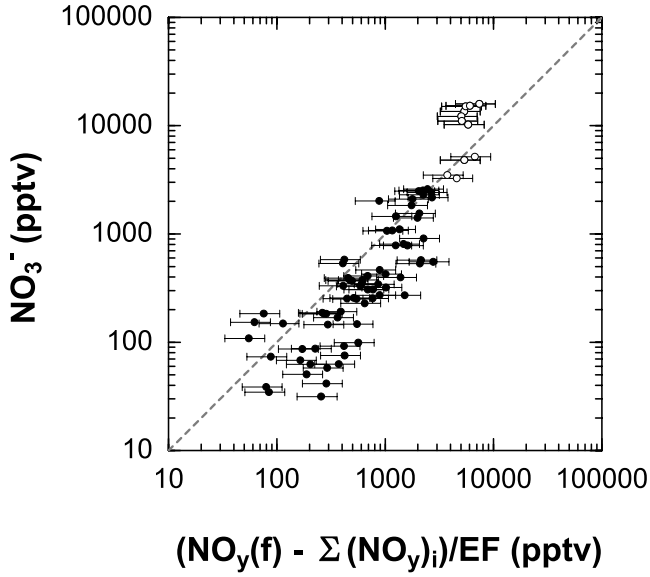

Figure 11. Scatterplot between NO_3^- and NO_3^- (L) = (NO_y (f) − $\sum(NO_y)_i$)/EF, where the EF (enhancement factor) is assumed to be 2. Open circles correspond to the data with $\Delta NO_y > 2500$ pptv, while solid circles correspond to $\Delta NO_y < 2500$ pptv. Error bars indicate the uncertainty in EF. The dashed line indicates the 1:1 line.

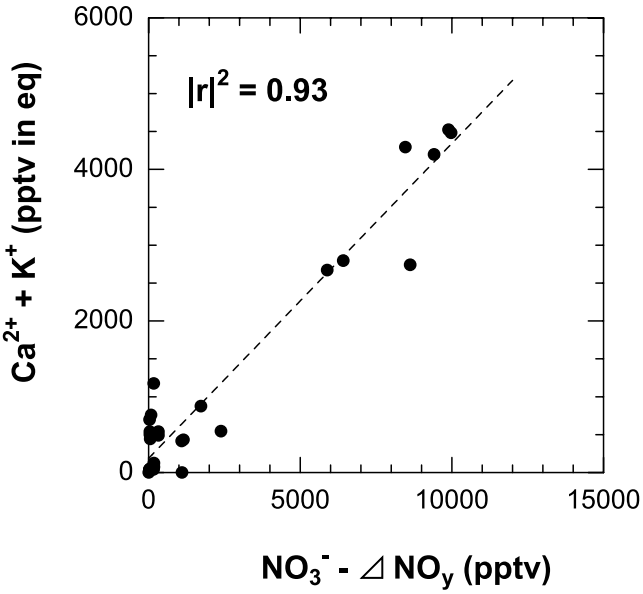

Figure 12. Scatterplot of the sum of Ca^{2+} and K^+ in equivalence and δNO_3^-. The dashed line represents the least squares best fit.

Ca^{2+} and K^+ in equivalence accounted for 20% and 25% of δNO_3^- on average, respectively, for ΔNO_y > 2500 pptv. Namely, $Ca(NO_3)_2$ and KNO_3, which are not measured as NO_y, can explain a maximum of 45% of the δNO_3^-. The remaining δNO_3^- (~35%), which cannot be explained by either larger NH_4NO_3 (D_p = 1.5–3 μm) or Ca^{2+} plus K^+ particles, is within the combined uncertainties of the measurements and EF.

5. Contribution of Particulate NO_3^- to the NO_y Budget Over the Western Pacific

[31] Finally, we investigated the partitioning between particulate NO_3^- and gas-phase NO_y. Figure 13 shows vertical profiles of NO_3^-, $\sum(NO_y)_i$, and $\sum(NO_y)_i + NO_3^-$ to NO_y ratios at 10°–30°N and 30°–45°N. The partitioning of individual NO_y compounds is summarized in Table 3. The NO_y mixing ratios were systematically higher by 10–30% than the sum of individual gas-phase NO_y compounds at 0–4 km. An important feature is that particulate NO_3^- contributed 10–30% of the measured NO_y at 0–4 km. On average, the particulate NO_3^- fraction of NO_y was largest (26–37%) at 0–2 km, which was comparable to that of gas-phase HNO_3 (24–32%) at the same altitude. The result indicates that the active conversion of HNO_3 to NO_3^- is important, and particulate NO_3^- may thus contribute a significant fraction (~50%) to total nitrate, especially at 0–2 km during the TRACE-P period. Although the data for ΔNO_y > 2500 pptv observed at 0–2 km are included in Figure 13, the fraction of these data was only <3% of the total. Therefore a majority of NO_3^- shown in the figure are particles detected by the NO_y instrument.

[32] At altitudes of 2–6 km, very low values of NO_3^-/NO_y (0.02–0.10) indicate that a large fraction of the NO_3^- was scavenged by cloud droplets during the vertical transport from lower altitudes (0–2 km) [*Koike et al.*, 2003; *Kondo et al.*, 2004]. Note that the NO_3^- concentrations discussed here are fine-mode fractions of the total particulate NO_3^-, which were obtained by the PILS having a 50% size cut of 1.3 μm. When we use the NO_3^- data obtained by the DC-8 filter samples, which measured particles with D_p up to 6 μm [*Dibb et al.*, 2002], particulate NO_3^- constituted 54% of the total nitrate on average, reaching a maximum of 72% at 0–2 km where observed particles were heavily influenced by dust during TRACE-P [*Jordan et al.*, 2003b].

[33] For gas-phase NO_y, 80–90% of the measured NO_y at 0–6 km is accounted for by NO_x (= NO + NO_2), PAN, and HNO_3. These values are similar to those in air masses influenced by continental surface emissions previously observed at 0–5 km over the western Pacific during the Pacific Exploratory Mission (PEM) West B in 1994 [*Kondo et al.*, 1997b]. It is noted that gas-phase HNO_3 was measured using a chemical ionization mass spectrometer (CIMS) onboard the P-3B during TRACE-P. During PEM-West B and TRACE-P, on the other hand, HNO_3 was measured by the University of New Hampshire's (UNH) mist chamber/ion chromatography (MC-IC) instrument onboard the DC-8 research aircraft. The UNH/MC-IC could sample nitrate-containing particles, as indicated by intercomparison between the two instruments during TRACE-P [*Zondlo et al.*, 2003]. Accordingly, the sampling by the UNH/MC-IC would result in higher measurements of gas-phase HNO_3 relative to the true amount. Thus much more accurate evaluations of the NO_y budget are enabled in this study by highly selective and sensitive measurements of gas-phase HNO_3 by the CIMS instrument and of particulate NO_3^- by the PILS-IC.

[34] PAN was systematically higher at 30°–45°N (175–930 pptv) than at 10°–30°N (140–190 pptv), consistent with its chemical stability at lower temperatures. Meanwhile, PPN (<6%) and alkyl nitrate (<5%) were minor compounds in the NO_y budget during TRACE-P. The

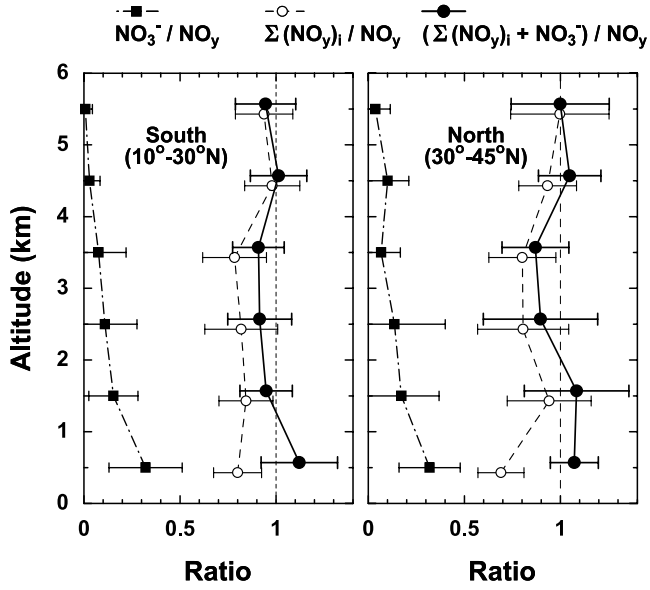

Figure 13. Vertical profiles of the mean values of NO_3^-/NO_y (solid squares), $\sum(NO_y)_i/NO_y$ (open circles), and $(\sum(NO_y)_i + NO_3^-)/NO_y$ (solid circles) at (left) 10°–30°N and (right) 30°–45°N.

Table 3. Reactive Nitrogen Budgets and Partitioning at 10°–30°N and 30°–45°N on Board P-3B During TRACE-P[a]

Altitude, km	Latitude[b]	NO_3^-, pptv	NO_x, pptv	HNO_3, pptv	PAN, pptv	PPN, pptv	Alkyl Nitrate, pptv	NO_y, pptv	$\Sigma(NO_y)_i + NO_3^-$, pptv
4–6	N	25 ± 42	34 ± 37	115 ± 81	174 ± 122	21 ± 19	15 ± 7	388 ± 238	359 ± 203
		(0.06 ± 0.12)	(0.08 ± 0.08)	(0.34 ± 0.20)	(0.47 ± 0.11)	(0.05 ± 0.02)	(0.05 ± 0.02)	(–)	(1.05 ± 0.23)
4–6	S	18 ± 18	30 ± 15	156 ± 70	143 ± 104	14 ± 10	9 ± 4	368 ± 174	437 ± 229
		(0.02 ± 0.04)	(0.08 ± 0.03)	(0.44 ± 0.16)	(0.35 ± 0.13)	(0.03 ± 0.01)	(0.03 ± 0.01)	(–)	(0.98 ± 0.16)
2–4	N	103 ± 408	70 ± 91	221 ± 139	438 ± 258	61 ± 38	30 ± 11	997 ± 628	883 ± 747
		(0.10 ± 0.21)	(0.07 ± 0.05)	(0.23 ± 0.14)	(0.46 ± 0.13)	(0.06 ± 0.02)	(0.04 ± 0.01)	(–)	(0.91 ± 0.29)
2–4	S	110 ± 237	63 ± 47	289 ± 308	160 ± 142	24 ± 13	15 ± 7	713 ± 655	889 ± 628
		(0.09 ± 0.16)	(0.10 ± 0.05)	(0.39 ± 0.17)	(0.21 ± 0.14)	(0.03 ± 0.02)	(0.04 ± 0.03)	(–)	(0.91 ± 0.15)
0–2	N	1761 ± 3199	1142 ± 4948	430 ± 316	928 ± 542	155 ± 91	63 ± 24	3836 ± 5865	3943 ± 4749
		(0.37 ± 0.39)	(0.16 ± 0.15)	(0.24 ± 0.20)	(0.33 ± 0.10)	(0.05 ± 0.02)	(0.03 ± 0.01)	(–)	(1.18 ± 0.34)
0–2	S	230 ± 432	146 ± 200	209 ± 222	189 ± 184	47 ± 34	34 ± 18	776 ± 624	1011 ± 556
		(0.26 ± 0.19)	(0.16 ± 0.10)	(0.32 ± 0.17)	(0.20 ± 0.12)	(0.05 ± 0.03)	(0.05 ± 0.03)	(–)	(1.06 ± 0.19)

[a]Values are mean ±1 σ. The numbers in parentheses are the ratios to the measured NO_y. The numbers of data points are within a range of 40–120 in each column.

[b]Latitudes 10°–30°N are denoted as S, and latitudes 30°–45°N are denoted as N.

present results emphasize that the contribution of particulate NO_3^- to NO_y should be taken into account when evaluating NO_y speciation and budget closure using an NO_y instrument with a catalytic converter, especially when near a large source region of particulate NO_3^-.

6. Conclusions

[35] The sum of individual NO_y gas components ($\sum(NO_y)_i$), NO_y, and particulate NO_3^- (D_p <1.3 μm) were measured simultaneously on board the P-3B aircraft at 10°–45°N over the western Pacific during TRACE-P. The inorganic chemical composition of aerosols, including NO_3^-, was measured by the PILS-IC technique. In addition to the field measurements, conversion efficiencies of particulate NH_4NO_3, KNO_3, $NaNO_3$, and $Ca(NO_3)_2$ by the gold tube catalytic converter were measured in the laboratory. NH_4NO_3 was converted to NO with an efficiency of 91 ± 9%, which was as high as that for HNO_3. Meanwhile, the conversion efficiencies of the aerosols in the other forms were as low as 1–3%. These results are consistent with the particulate NO_3^- measurements made on board the aircraft.

[36] Elevated NO_3^- was typically observed within biomass/biofuel burning plumes at 0–4 km. The measured NO_y was systematically higher by 10–30% than the $\sum(NO_y)_i$ at 0–4 km. Under low dust loadings with $[Ca^{2+}]$ < 200 pptv, the observed particles reside mostly in the fine mode, while the size distributions showed bimodal distribution within the fine and coarse modes under high dust loadings ($[Ca^{2+}]$ > 400 pptv). The $\Delta NO_y = NO_y - \sum(NO_y)_i$ values were approximately equal to NO_3^- concentrations under low dust loadings, suggesting that the NO_y instrument quantitatively converted NO_3^- to NO. More than 44% of the NO_3^- detected by the NO_y instrument was estimated to be in the form of NH_4NO_3, which was identified from the measured ionic composition of the aerosols.

[37] NO_3^- far exceeded ΔNO_y only in polluted air masses with high dust loadings at 0–2 km over the Yellow Sea (30°–45°N). By using the forward facing NO_y inlet, 20% of the excess NO_3^- ($\delta NO_3^- = NO_3^- - \Delta NO_y$) was estimated to be mainly in the form of NH_4NO_3, suggesting that the size of this NO_3^- particle species detected by PILS-IC was in the range of D_p = 1.5–3 μm, which was larger than the size cutoff of the rearward facing NO_y instrument. Some of the other δNO_3^- can be in the form of $Ca(NO_3)_2$ (<20%) and KNO_3 (<25%) under high dust loading with a mixture of anthropogenic pollution, considering the measured aerosol ion composition. Particulate NO_3^- in these forms can partly explain the large δNO_3^-, because their conversion in the NO_y instrument is negligible. The remaining δNO_3^- (~35%), which cannot be explained either by larger NH_4NO_3 (D_p = 1.5–3 μm) or $Ca^{2+} + K^+$ particles, is within the combined uncertainties of the measurements and the enhancement factor for the forward facing NO_y inlet.

[38] Generally, the contribution of particulate NO_3^- to NO_y was most important at 0–2 km, where the NO_3^- concentrations constituted 10–30% of NO_y. On average, the concentrations of NO_3^- and gas-phase HNO_3 were comparable in this region. These results indicate the importance of properly including particulate NO_3^- in assessing the budget of reactive nitrogen using measurements of NO_y by the catalytic conversion technique, especially when near a large source region of particulate NO_3^-.

[39] **Acknowledgments.** The TRACE-P mission was supported by the NASA Global Tropospheric Chemistry Program. The authors wish to thank the crew of the NASA P-3B aircraft for their support. M. Kanada and N. Toriyama are greatly appreciated for their technical assistance with the measurements of NO, NO_2, and NO_y. A. Yamazaki is appreciated for his assistance with the data analysis. Y.M. was supported by research fellowships of the Japan Society for the Promotion of Science for Young Scientists.

References

Brasseur, G. P., J. J. Orlando, and G. S. Tyndall (1999), *Atmospheric Chemistry and Global Change*, Oxford Univ. Press, New York.

Chameides, W. L., et al. (1992), Ozone precursor relationships in the ambient atmosphere, *J. Geophys. Res.*, *97*, 6037–6055.

Clarke, A. D., et al. (2004), Size-distributions and mixtures of dust and black carbon aerosol in Asian outflow: Physiochemistry and optical properties, *J. Geophys. Res.*, *109*, D15S09, doi:10.1029/2003JD004378.

Crutzen, P. J. (1979), The role of NO and NO_2 in the chemistry of the troposphere and stratosphere, *Annu. Rev. Earth Planet. Sci.*, *7*, 443–472.

Day, D. A., M. B. Dillon, P. J. Wooldridge, J. A. Thornton, R. S. Rosen, E. C. Wood, and R. C. Cohen (2003), On alkyl nitrates, O_3, and the "missing NO_y," *J. Geophys. Res.*, *108*(D16), 4501, doi:10.1029/2003JD003685.

DeCarlo, P. F., J. G. Slowik, D. R. Worsnop, P. Davidovits, and J. L. Jimenez (2004), Particle morphology and density characterization by combined mobility and aerodynamic diameter measurements. part 1: Theory, *Aerosol Sci. Technol.*, *38*, 1185–1205.

Dibb, J. E., R. W. Talbot, G. Seid, C. Jordan, E. Scheuer, E. Atlas, N. J. Blake, and D. R. Blake (2002), Airborne sampling of aerosol particles: Comparison between surface sampling at Christmas Island and P-3 sam-

pling during PEM Tropics B, *J. Geophys. Res.*, *107*(D2), 8230, doi:10.1029/2001JD000408.
Durham, M. D., and D. A. Lundgren (1980), Evaluation of aerosol aspiration efficiency as a function of Stokes number, velocity ratio and nozzle angle, *J. Aerosol Sci.*, *11*, 179–188.
Fahey, D. W., C. S. Eubank, G. Hübler, and F. C. Fehsenfeld (1985), Evaluation of a catalytic reduction technique for the measurement of total reactive odd-nitrogen NO_y in the atmosphere, *J. Atmos. Chem*, *3*, 435–468.
Fahey, D. W., et al. (1989), In-situ measurements of total reactive nitrogen, total water, and aerosol in a polar stratospheric cloud in the Antarctic, *J. Geophys. Res.*, *94*, 11,299–11,315.
Fahey, D. W., et al. (2001), The detection of large HNO_3-containing particles in the winter Arctic stratosphere, *Science*, *291*, 1026–1031.
Feigl, C., et al. (1999), Observation of NO_y uptake by particles in the Arctic tropopause region at low temperatures, *Geophys. Res. Lett.*, *26*, 2215–2218.
Hübler, G., D. W. Fahey, B. A. Ridley, G. L. Gregory, and F. C. Fehsenfeld (1992), Airborne measurements of total reactive odd nitrogen (NO_y), *J. Geophys. Res.*, *97*, 9833–9850.
Jayne, J. T., D. C. Leard, X. F. Zhang, P. Davidovits, K. A. Smith, C. E. Kolb, and D. R. Worsnop (2000), Development of an aerosol mass spectrometer for size and composition analysis of submicron particles, *Aerosol Sci. Technol.*, *33*, 49–70.
Jordan, C. E., et al. (2003a), Chemical and physical properties of bulk aerosols within four sectors observed during TRACE-P, *J. Geophys. Res.*, *108*(D21), 8813, doi:10.1029/2002JD003337.
Jordan, C. E., J. E. Dibb, B. E. Anderson, and H. E. Fuelberg (2003b), Uptake of nitrate and sulfate on dust aerosols during TRACE-P, *J. Geophys. Res.*, *108*(D20), 8817, doi:10.1029/2002JD003101.
Koike, M., et al. (2000), Impact of aircraft emissions on reactive nitrogen over the North Atlantic flight corridor region, *J. Geophys. Res.*, *105*, 3665–3677.
Koike, M., et al. (2003), Export of anthropogenic reactive nitrogen and sulfur compounds from the east Asia region in spring, *J. Geophys. Res.*, *108*(D20), 8789, doi:10.1029/2002JD003284.
Kondo, Y., S. Kawakami, M. Koike, D. W. Fahey, H. Nakajima, N. Toriyama, M. Kanada, Y. Zhao, G. W. Sachse, and G. L. Gregory (1997a), The performance of an aircraft instrument for the measurement of NO_y, *J. Geophys. Res.*, *102*, 28,663–28,671.
Kondo, Y., M. Koike, S. Kawakami, H. B. Singh, H. Nakajima, G. L. Gregory, D. R. Blake, G. W. Sachse, J. T. Merrill, and R. E. Newell (1997b), Profiles and partitioning of reactive nitrogen over the Pacific Ocean in winter and early spring, *J. Geophys. Res.*, *102*, 28,405–28,424.
Kondo, Y., et al. (2003), Uptake of reactive nitrogen on cirrus cloud particles in the upper troposphere and lowermost stratosphere, *Geophys. Res. Lett.*, *30*(4), 1154, doi:10.1029/2002GL016539.
Kondo, Y., et al. (2004), Impacts of biomass burning in Southeast Asia on ozone and reactive nitrogen over the western Pacific in spring, *J. Geophys. Res.*, *109*, D15S12, doi:10.1029/2003JD004203.
Lawrence, M. G., and P. J. Crutzen (1998), The impact of cloud particle gravitational settling on soluble trace gas distributions, *Tellus, Ser. B*, *50*, 263–289.
Liu, S. C., M. Trainer, F. C. Fehsenfeld, D. D. Parrish, E. J. Williams, D. W. Fahey, G. Huber, and P. C. Murphy (1987), Ozone production in the rural troposphere and the implications for regional and global ozone distributions, *J. Geophys. Res.*, *92*, 4191–4207.
Ma, Y., et al. (2003), Characteristics and influence of biosmoke on the fine-particle ionic composition measured in Asian outflow during the Transport and Chemical Evolution over the Pacific (TRACE-P) experiment, *J. Geophys. Res.*, *108*(D21), 8816, doi:10.1029/2002JD003128.
Ma, Y., et al. (2004), Intercomparison of airborne measurements of aerosol ionic chemical composition during TRACE-P and ACE-Asia, *J. Geophys. Res.*, *109*, D15S06, doi:10.1029/2003JD003673.
Miyazaki, Y., et al. (2003), Synoptic-scale transport of reactive nitrogen over the western Pacific in spring, *J. Geophys. Res.*, *108*(D20), 8788, doi:10.1029/2002JD003248.
Neuman, J. A., et al. (2002), Fast-response airborne in situ measurements of HNO3 during the Texas Air Quality Study, *J. Geophys. Res.*, *107*(D20), 4436, doi:10.1029/2001JD001437.
Neuman, J. A., et al. (2003), Variability in ammonium nitrate formation and nitric acid depletion with altitude and location over California, *J. Geophys. Res.*, *108*(D17), 4557, doi:10.1029/2003JD003616.
Orsini, D. A., Y. Ma, A. Sullivan, B. Sierau, K. Baumann, and R. J. Weber (2003), Refinements to the particle-into-liquid sampler (PILS) for ground and airborne measurements of water soluble aerosol composition, *Atmos. Environ.*, *37*, 1243–1259.
Parrish, D. D., et al. (2004), Fraction and composition of NO_y transported in air masses lofted from the North American continental boundary layer, *J. Geophys. Res.*, *109*, D09302, doi:10.1029/2003JD004226.
Reid, J. S., and P. V. Hobbs (1998), Physical and optical properties of young smoke from individual biomass fires in Brazil, *J. Geophys. Res.*, *103*, 32,013–32,030.
Ridley, B. A., J. G. Walega, J. E. Dye, and F. E. Grahek (1994), Distributions of NO, NO_x, NO_y, and O_3 to 12 km altitude during the summer monsoon season over New Mexico, *J. Geophys. Res.*, *99*, 25,519–25,534.
Ryerson, T. B., et al. (2003), Effect of petrochemical industrial emissions of reactive alkenes and NO_x on tropospheric ozone formation in Houston, Texas, *J. Geophys. Res.*, *108*(D8), 4249, doi:10.1029/2002JD003070.
Sandholm, S. T., et al. (1994), Summertime partitioning and budget of NO_y, compounds in the troposphere over Alaska and Canada: ABLE 3B, *J. Geophys. Res.*, *99*, 1837–1861.
Savoie, D. L., and J. M. Prospero (1982), Particle size distribution of nitrate and sulfate in the marine atmosphere, *Geophys. Res. Lett.*, *9*, 1207–1210.
Seinfeld, J. H., and S. N. Pandis (1998), *Atmospheric Chemistry and Physics: From Air Pollution to Climate Change*, John Wiley, Hoboken, N. J.
Singh, H. B., et al. (2003), In situ measurements of HCN and CH_3CN over the Pacific Ocean: Sources, sinks, and budgets, *J. Geophys. Res.*, *108*(D20), 8795, doi:10.1029/2002JD003006.
Solomon, S., et al. (1986), On the depletion of Antarctic ozone, *Nature*, *321*, 755–758.
Swietlicki, E., et al. (2000), Hygroscopic properties of aerosol particles in the north-eastern Atlantic during ACE-2, *Tellus, Ser. B*, *52*, 201–227.
Talbot, R. W., et al. (1999), Reactive nitrogen budget during the NASA SONEX mission, *Geophys. Res. Lett.*, *26*, 3057–3060.
Warneck, P. (1988), *Chemistry of the Natural Atmosphere*, Elsevier, New York.
Weber, R. J., D. Orsini, Y. Daun, Y.-N. Lee, P. J. Klotz, and F. Brechtel (2001), A particle-into-liquid collector for rapid measurement of aerosol bulk chemical composition, *J. Aerosol Sci. Technol.*, *35*, 718–727.
Weber, R. J., et al. (2003), New particle formation in anthropogenic plumes advecting from Asia observed during TRACE-P, *J. Geophys. Res.*, *108*(D21), 8814, doi:10.1029/2002JD003112.
Weinheimer, A. J., et al. (1998), Uptake of NO_y on wave-cloud ice particles, *Geophys. Res. Lett.*, *25*, 1725–1728.
Wolff, G. T. (1984), On the nature of nitrate and in coarse continental aerosols, *Atmos. Environ.*, *18*, 977–981.
Zondlo, M. A., R. L. Mauldin, E. Kosciuch, C. A. Cantrell, and F. L. Eisele (2003), Development and characterization of an airborne-based instrument used to measure nitric acid during the NASA Transport and Chemical Evolution over the Pacific field experiment, *J. Geophys. Res.*, *108*(D20), 8793, doi:10.1029/2002JD003234.

D. R. Blake, Department of Chemistry, University of California, Irvine, Irvine, CA 92697, USA. (drblake@uci.edu)
A. D. Clarke and V. N. Kapustin, School of Ocean and Earth Science and Technology, University of Hawaii at Manoa, Honolulu, HI 96822, USA. (tclarke@soest.hawaii.edu; kapustin@soest.hawaii.edu)
F. L. Eisele, F. Flocke, and A. J. Weinheimer, Atmospheric Chemistry Division, National Center for Atmospheric Research, Boulder, CO 80303, USA. (eisele@ucar.edu; ffl@ucar.edu; wein@ucar.edu)
M. Fukuda, Y. Kondo, Y. Miyazaki, and N. Takegawa, Research Center for Advanced Science and Technology, University of Tokyo, 4-6-1 Komaba, Meguro-ku, Tokyo 153-8904, Japan. (fukuda@atmos.rcast.u-tokyo.ac.jp; kondo@atmos.rcast.u-tokyo.ac.jp; yuzom@atmos.rcast.u-tokyo.ac.jp; takegawa@atmos.rcast.u-tokyo.ac.jp)
K. Kita, Department of Environmental Science, Ibaraki University, Bunkyo 2-1-1, Mito, Ibaraki 310-8512, Japan. (kita@env.sci.ibaraki.ac.jp)
M. Koike, Earth and Planetary Science, Graduate School of Science, University of Tokyo, Tokyo 113-0033, Japan. (koike@eps.s.u-tokyo.ac.jp)
B. Liley, National Institute of Water and Atmospheric Research, Lauder, PB 50061 Omakau, Central Otago 9182, New Zealand. (b.liley@niwa.co.nz)
Y. Ma, Department of Civil and Environmental Engineering, Duke University, Durham, NC 27708-0287, USA. (yilinma@duke.edu)
R. J. Weber, School of Earth and Atmospheric Sciences, Georgia Institute of Technology, Atlanta, GA 30332-0340, USA. (rweber@eas.gatech.edu)
M. A. Zondlo, Southwest Sciences, Inc., 1570 Pacheco Street, Suite E-11, Santa Fe, NM 87505, USA. (mzondlo@swsciences.com)